Journal of Guidance, Control, and Dynamics
Vol. 42, No. 3, March 2019

Check for updates

Engineering Notes

Solar-Powered Aircraft Endurance Map

Jianfa Wu* and Honglun Wang†
Beihang University, 100191 Beijing, People's Republic of China
Yu Huang‡
Tsinghua University, 100084 Beijing, People's Republic of China
Menghua Zhang§
Beihang University, 100191 Beijing, People's Republic of China
and
Zikang Su¶
Nanjing University of Aeronautics and Astronautics, 211106 Nanjing, People's Republic of China

DOI: 10.2514/1.G003704

I. Introduction

SOLAR-POWERED aircrafts (SAs) maintain flight by transforming solar irradiance into energy using solar cells. As a consequence of their excellent duration, SAs are suitable for some long-endurance daytime and nighttime missions [1–5], such as those that involve target tracking, area surveillance, and communications relay. Before designing flight trajectories or energy management strategies for such missions, the endurance performance of SA should first be considered to guarantee that sufficient energy will be available to complete the necessary maneuvers in the mission area.

However, to the best of our knowledge, relatively little specialized research has been conducted on the SA endurance evaluation index and corresponding methodology; instead, most studies have focused on SA energy modeling [6–10], trajectory optimization [6,7,9–11], and energy management strategies [1,8,11,12] or the traditional electric aircraft (EA) endurance evaluation [13–16]. For the EA endurance evaluation, it is relatively easy to estimate the maximum endurance time or range of EA, because the capacity of an airborne battery is relatively certain and nearly unaffected by the geographical location. Therefore, the flight time or range is generally selected as the evaluation index. Unlike EAs, the SA endurance performance is not only related to the battery capacity but also depends on the incident solar irradiance, which is closely related to the current geographical location of the SA [17]. Accordingly, when SAs execute cross-regional flight missions (i.e., when there are obvious changes in the longitude and latitude during flight), the energy production status will vary with the location, making it difficult to resolve the maximum endurance time. Therefore, traditional endurance evaluation methods for EAs are not suitable for SAs. For the SA endurance, recent studies have explored the energy balance problem in steady-state cruise [18–21]. Unfortunately, neither a unified standard for the evaluation index nor an explicit quantifiable evaluation method has been proposed.

In addition, the external environment can vary greatly during cross-regional flight due to the large time span and spatial extent. According to the thermal equilibrium principle for solar photovoltaic modules, the solar cell photoelectric efficiency can be influenced by external environmental factors (e.g., the temperature and air density) [22]. Therefore, the variable efficiency can also influence the endurance performance. However, most previous studies that conduct the SA energy modeling restrict SA flights to a small-scale region [6–12] in which the location parameters (i.e., the longitude, latitude, and even flight altitude [6,9,10]) and the corresponding solar irradiation parameters can be regarded as constants, thereby neglecting the influences of the external environment on the SA energy production, for example, the variable photoelectric efficiency.

Based on the above analysis, proposed solutions for SA endurance evaluation problems should meet the following requirements:

1) The designed evaluation index should be capable of visually reflecting the endurance performance when SAs execute cross-regional flight missions. In addition, the calculation method should be relatively straightforward and simple.

2) The evaluation method should be able to reflect the influences of changes in the geographical location and environmental factors on the SA endurance performance during cross-regional flight missions.

Based on these requirements, inspired by map-based research methods in geography (e.g., precipitation and air temperature distribution maps) [23–25], a visualization methodology called the SA endurance map is proposed for the first time in this Note to intuitively evaluate the SA endurance performance in the mission area. The main contributions are as follows. First, considering the influences of external environmental factors, the variable solar cell efficiency is introduced to satisfy the requirements of the SA endurance evaluation. Then, according to the variable efficiency, the 24-hour flight net energy is resolved and employed as the endurance evaluation index rather than the endurance time or range. On this basis, to reflect the influence of the large spatial extent in the cross-regional flight mission on the net energy distribution, the net energy distribution is expressed in the form of a map, that is, the proposed SA endurance map. Finally, typical relevant applications of the SA endurance map are further expanded and discussed.

II. Methodology

The method used to draw the SA endurance map is summarized as follows. First, a solar irradiance model is established according to all of the sampling site data from the American Society of Heating, Refrigerating and Air-Conditioning Engineers (ASHRAE) Clear Sky Model [26,27] in the mission area. Second, the variable solar cell photoelectric efficiency at each sampling site is introduced according to the environmental factors at each site. Third, 24-hour SA energy harvesting and consumption models are established according to the abovementioned variable efficiency and solar irradiance model. Finally, Kriging interpolation for the 24-hour net energy value at each sampling site is conducted to construct the net energy distribution map, that is, the proposed SA endurance map.

Received 20 March 2018; revision received 30 August 2018; accepted for publication 6 September 2018; published online 23 November 2018.

*Ph.D. Student, School of Automation Science and Electrical Engineering, Shenyuan Honor College of Beihang University; jianfa_wu@163.com.

†Professor, School of Automation Science and Electrical Engineering, Science and Technology on Aircraft Control Laboratory; wang_hl_12@126.com, hl_wang_2002@126.com (Corresponding Author).

‡Postdoctor, Institute of Public Safety Research; hy5154@163.com.

§Master Student, School of Automation Science and Electrical Engineering; zmh_117@163.com.

¶Lecturer, College of Automation Engineering; szkbeyond@126.com.

Considering practical engineering applications, the aircraft performance should be evaluated under a relatively ideal environment and flight state, which is the consensus for most studies on endurance evaluation [13–16,18–21]. Therefore, the following assumptions should be maintained before constructing the endurance map:

Assumption 1: The wind speed is assumed to be much lower than the SA flight speed. Thus, the influence of the wind on the SA energy production and consumption can be neglected.

Assumption 2: For the endurance evaluation, the SA is assumed to be flying in steady-state cruise mode (i.e., at constant altitude and speed). Furthermore, the additional energy consumption, except for that during steady-state cruise, is neglected.

A. Solar Irradiance Received by SA

The ASHRAE Clear Sky Model, which is widely applied in solar engineering because of its low computational complexity and high accuracy, is introduced for the solar irradiance modeling as follows:

$$\begin{cases} P_{\mathrm{SA}} = P_b + P_d + P_r \\ P_b = I_b \sin \alpha_e \\ P_d = I_d \\ P_r = 0 \end{cases} \tag{1}$$

where P_{SA} is the solar irradiance received on the wing surface of SA; P_b, P_d, and P_r are the beam, diffuse, and ground reflection components in P_{SA}, respectively; α_e is the solar elevation angle; and I_b and I_d are the beam and diffuse irradiances incident on the Earth horizontal surface, respectively, whose values depend on the corresponding optical depths τ_b and τ_d as follows:

$$\begin{cases} I_b = I \exp(-\tau_b m_r^b) \\ I_d = I \exp(-\tau_d m_r^d) \\ I = I_0 \left(1 + 0.034 \cos \dfrac{2\pi n_{\mathrm{day}}}{365.25} \right) \\ b = 1.219–0.043\tau_b - 0.151\tau_d - 0.204\tau_b\tau_d \\ d = 0.202 + 0.852\tau_b - 0.007_d - 0.357\tau_b\tau_d \\ m_r = \dfrac{1}{\sin \alpha_e} \end{cases} \tag{2}$$

where I is the solar irradiance perpendicular to the horizontal plane in the exoatmosphere; $I_0 = 1367\ \mathrm{W/m^2}$ is the solar constant; n_{day} is the number of solar days starting from January 1; b and d are the beam and diffuse air mass exponents, respectively; and m_r is the air mass ratio.

The optical depths τ_b and τ_d are obtained according to years of engineering practice and tabulated by the ASHRAE Handbook [26]. Different sampling sites in the ASHRAE Clear Sky Model have different pairs of τ_b and τ_d. In the same site, the pair of τ_b and τ_d in each month are different from those in other months.

B. Modified SA Energy Production Model

When sunlight shines on solar cells located on the wings of SA, the solar cells produce an electric power, P_{in}:

$$P_{\mathrm{in}} = \eta_{\mathrm{sol}} \mathrm{SP}_{\mathrm{SA}} \tag{3}$$

where η_{sol} is the solar cell efficiency and S is the area of the wing.

In previous investigations involving the SA energy production modeling, η_{sol} is mostly regarded as a constant. However, η_{sol} can be greatly influenced by the operating temperature of the photovoltaic module; therefore, it is calculated by the following modified expression [28]:

$$\eta_{\mathrm{sol}} = [1 + (T_{\mathrm{sol}} - 25)\alpha_\eta]\eta_{\mathrm{sol}}^{\mathrm{STC}} \tag{4}$$

where $\eta_{\mathrm{sol}}^{\mathrm{STC}}$ is the nominal solar energy conversion efficiency under standard testing conditions (air mass: AM 1.5; photovoltaic module temperature: 25°C; and solar irradiance: $1000\ \mathrm{W/m^2}$); α_η is the temperature correction factor; and T_{sol} is the current photovoltaic module temperature, which can be analyzed according to the principle of thermal equilibrium, the SA configuration, the airspeed, and the flight altitude as described below.

The solar radiation energy absorbed by a photovoltaic module can be converted into three components: the electrical energy, the energy corresponding to thermal radiation, and the energy corresponding to heat convection. When the photovoltaic module is in a steady-working state, the principle of thermal equilibrium of the photovoltaic module can be expressed as follows [22]:

$$\alpha_{\mathrm{sol}} P_{\mathrm{SA}} = \eta_{\mathrm{sol}} P_{\mathrm{SA}} + \varepsilon_{\mathrm{sol}} \sigma (T_{\mathrm{sol}}^4 - T_{\mathrm{sky}}^4) + C_{\mathrm{the}} (T_{\mathrm{sol}} - T_{\mathrm{atm}}) \tag{5}$$

where α_{sol} is the absorption rate of the photovoltaic module; $\varepsilon_{\mathrm{sol}}$ is the thermal radiation emissivity of the photovoltaic module; s the Stefan–Boltzmann constant; T_{sky} is the effective sky temperature; T_{atm} is the atmospheric environment temperature at the current flight altitude; and C_{the} is the convective heat transfer coefficient.

Remark 1: To guarantee the reliability of the photovoltaic module, the internal heat generation of the related circuit is well controlled in the design process. Thus, the internal heat generation of the photovoltaic module can be ignored in Eq. (5). The photovoltaic modules on the wings are rigidly connected to the bottom both through internal supports and through connections at the edges. Because these connections have relatively small cross-sectional areas, the heat transfer through them can also be neglected in Eq. (5) [29].

The value of T_{sky} in Eq. (5) is calculated as follows [30]:

$$T_{\mathrm{sky}} = 0.0552 T_{\mathrm{atm}}^{1.5} \tag{6}$$

Considering the elevation of the site, T_{atm} is calculated according to the following empirical formula:

$$T_{\mathrm{atm}} = \begin{cases} T_{\mathrm{ma}} - 0.0065(z - z_{\mathrm{local}}), & z \le 11000\ \mathrm{m} \\ T_{\mathrm{ma}} - 71.5 + 0.0065 z_{\mathrm{local}}, & 11000\ \mathrm{m} < z \le 20000\ \mathrm{m} \\ T_{\mathrm{ma}} - 71.5 + 0.0065 z_{\mathrm{local}} + 0.001(z - 20000), & 20000\ \mathrm{m} < z \le 30000\ \mathrm{m} \end{cases} \tag{7}$$

where z is the flight altitude; z_{local} is the elevation of the site; and T_{ma} is the measured air temperature on the ground.

The value of C_{the} in Eq. (5) is calculated as follows [30]:

$$\begin{cases} C_{\mathrm{the}} = \dfrac{\lambda_{\mathrm{air}} N_u}{c} \\ N_u = \begin{cases} 0.664 Re^{0.5} Pr^{1/3} & Re \le 5 \times 10^5 \\ (0.037 Re^{0.8} - 871) Pr^{1/3} & Re > 5 \times 10^5 \end{cases} \\ Re = \dfrac{\rho V c}{\mu_{\mathrm{air}}} \\ Pr = \dfrac{c_p \mu_{\mathrm{air}}}{\lambda_{\mathrm{air}}} \\ \mu_{\mathrm{air}} = \left(\dfrac{T_{\mathrm{sky}}}{288.15}\right)^{1.5} \dfrac{288.15+110.4}{T_{\mathrm{sky}}+110.4} \mu_0 \end{cases} \tag{8}$$

where λ_{air} is the air heat conductivity coefficient; c is the wing chord; N_u is the Nusselt number; Re is the Reynolds number; V is the airspeed; ρ is the air density, whose calculation method is provided by the International Standard Atmosphere (ISA, ISO 2533: 1975); Pr is the Prandtl number; $c_p = 1.003 \times 10^3$ J/(kg · K) is the specific heat at constant pressure; μ_{air} is the air viscosity coefficient; and μ_0 is the dry air viscosity coefficient at 288.15 K tabulated by the ISA.

Combining Eqs. (4) and (6–8) with the known solar cell parameters, α_{sol}, α_η, $\varepsilon_{\mathrm{sol}}$, and $\eta_{\mathrm{sol}}^{\mathrm{STC}}$, Eq. (5) can become a quartic equation with a single unknown variable, T_{sol}, which can be resolved by numerical algorithms. Then, the resolved T_{sol} can be substituted into Eq. (4), and the obtained η_{sol} can be used in Eq. (3). According to Eqs. (4–8), solar cell efficiencies at different flight altitudes and air temperatures can be obtained, as shown in Figs. 1 and 2, respectively. The corresponding solar cell and SA configuration parameters are shown in Table 1.

Table 1 Solar cell and SA configuration parameters

Parameter	Value
α_{sol}	0.92
$\varepsilon_{\mathrm{sol}}$	0.85
α_η	−0.38%
$\eta_{\mathrm{sol}}^{\mathrm{STC}}$	0.19
S, m^2	20.25
c, m	0.9
m, kg	37
R_a	25
ε	0.992
η_{prop}	0.85
η_{mot}	0.85
η_{ctrl}	0.95
C_{D0}	0.005

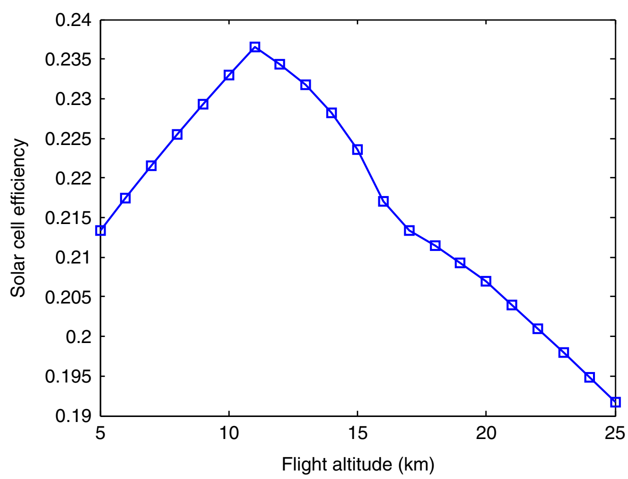

Fig. 1 Solar cell efficiencies at different altitudes.

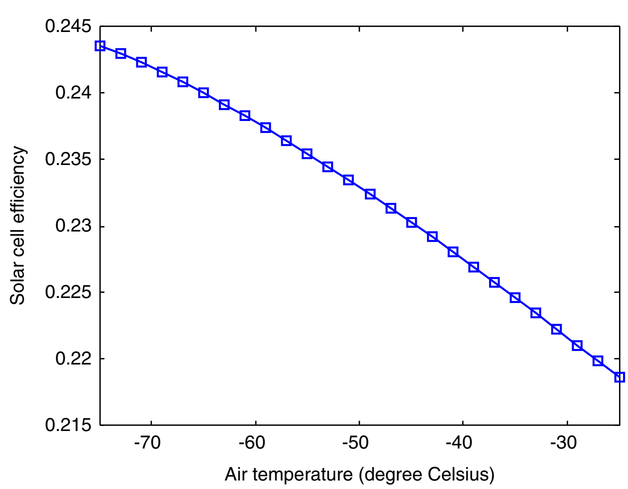

Fig. 2 Solar cell efficiencies at different air temperatures.

In Fig. 1, when the SA is located in the troposphere, the solar cell efficiency increases with the increasing flight altitude. In contrast, when the SA is located in the stratosphere, the solar cell efficiency decreases with the increasing flight altitude. At different flight altitudes, the efficiency can change by as much as 20–30%, which has a significant impact on the energy production. In Fig. 2, the efficiency strictly decreases with the increasing air temperature, and the maximum change in the efficiency can exceed 10%. In summary, for the SA endurance evaluation problem in the cross-regional flight mission, the influences of the external environment on the solar cell efficiency cannot be ignored.

The produced energy is expressed as follows:

$$E_{\mathrm{in}} = \int_{t_0}^{t_f} P_{\mathrm{in}}\, \mathrm{d}t \tag{9}$$

C. SA Energy Consumption Model

Assuming a quasi-static equilibrium flight, the energy consumption power P_{out} is calculated as follows:

$$\begin{cases} P_{\mathrm{out}} = \dfrac{TV}{\eta_{\mathrm{prop}} \eta_{\mathrm{mot}} \eta_{\mathrm{ctrl}}} \\ T = D \\ D = \dfrac{1}{2} \rho V^2 S C_D \\ C_D = C_{D0} + \dfrac{C_L^2}{\varepsilon \pi R_a} \\ C_L = \dfrac{2\ \mathrm{mg}}{\rho V^2 S} \end{cases} \tag{10}$$

where η_{prop}, η_{mot}, and η_{ctrl} are the efficiencies of the propeller, motor, and actuator, respectively; T is the thrust; D is the drag; C_D is the coefficient of drag; C_{D0} is the parasitic drag coefficient; C_L is the coefficient of lift; ε is the Oswald efficiency factor; and R_a is the ratio of the wing.

The consumed energy is as follows:

$$E_{\mathrm{out}} = \int_{t_0}^{t_f} P_{\mathrm{out}}\, \mathrm{d}t \tag{11}$$

Table 2 Initial mission parameters

Mission area	Mainland China and its offshore area, 396 sites [26]
Mission date	January 1, 2018, or March 21, 2018
Mission flight altitude, km	10; 15; 20; 25
Mission flight speed, m/s	30
Measured air temperature on the ground, T_{ma}	24-hour data comes from Meteorological Data Center, China Meteorological Administration (http://data.cma.cn/data/online/t/1) to simulate the meteorological forecasting results in step 1.
Simulation step size, min	1

D. SA Endurance Map

The SA endurance map for a future flight mission can be obtained through the following steps.

Step 1: Parameter initialization. The mission area, date, flight altitude, cruising speed, and solar cell and SA configuration parameters are first determined. Then, according to [26], all of the site information throughout the mission area, including the site locations, related sunrise/sunset times, and irradiance parameters (τ_b and τ_d), is obtained. Finally, the 24-hour temperature condition at each site after the start of the mission date is obtained through the meteorological forecasting.

Step 2: Available net energy calculation. First, the solar cell efficiency at each site is obtained using Eqs. (3–7) according to the flight altitude and the related atmospheric parameters (e.g., the air density, the thermodynamic coefficients, and the predicted temperature for each hour obtained from the meteorological forecasting). Then, the 24-hour produced energy at each site E_{in}^{24h} is calculated using Eqs. (1), (2), and (8) according to the related solar cell efficiency, sunrise/sunset times, and irradiance parameters. The 24-hour consumed energy at each site E_{out}^{24h} is calculated using Eqs. (9) and (10). Finally, the 24-hour available net energy at each site E_{net}^{24h} as the endurance evaluation index is determined by $E_{\text{net}}^{24h} = E_{\text{in}}^{24h} - E_{\text{out}}^{24h}$. The net energy directly reflects the integrated effect of the energy production and consumption. The more net energy the SA has, the better its endurance performance and its ability to execute complex maneuvers. Moreover, SAs can theoretically maintain nonstop flight only when the value of the 24-hour net energy is greater than zero.

Remark 2: E_{net}^{24h}, which is the theoretical maximum value of the energy available within a 24-hour period, contains not only the electrical energy stored in batteries but also the mechanical energy, including the gravitational potential energy and the kinetic energy. The battery parameters (e.g., the capacity and the energy density) can limit only the total amount of electrical energy that an SA can acquire. When the batteries in an SA are fully charged, the SA can either gradually climb to a higher altitude using advanced energy management strategies to transform the produced solar energy, which is calculated using Eqs. (3) and (9) and cannot be stored in batteries, into gravitational potential energy for storage or increase the motor speed to store the corresponding kinetic energy [1,7,8,11,12]. In this way, the total stored energy (i.e., the net energy) does not change. Therefore, the battery parameters do not need to be considered in the proposed endurance index.

Step 3: Net energy data interpolation. An interpolation operation for the net energy E_{net}^{24h} at each site is conducted to obtain the SA endurance map. In this Note, Kriging interpolation, which is widely used in the fields of geography and topography, is selected because of its excellent precision for nonuniform sampling points [23].

Step 4: The endurance map is updated (return to step 1) with an increase in time.

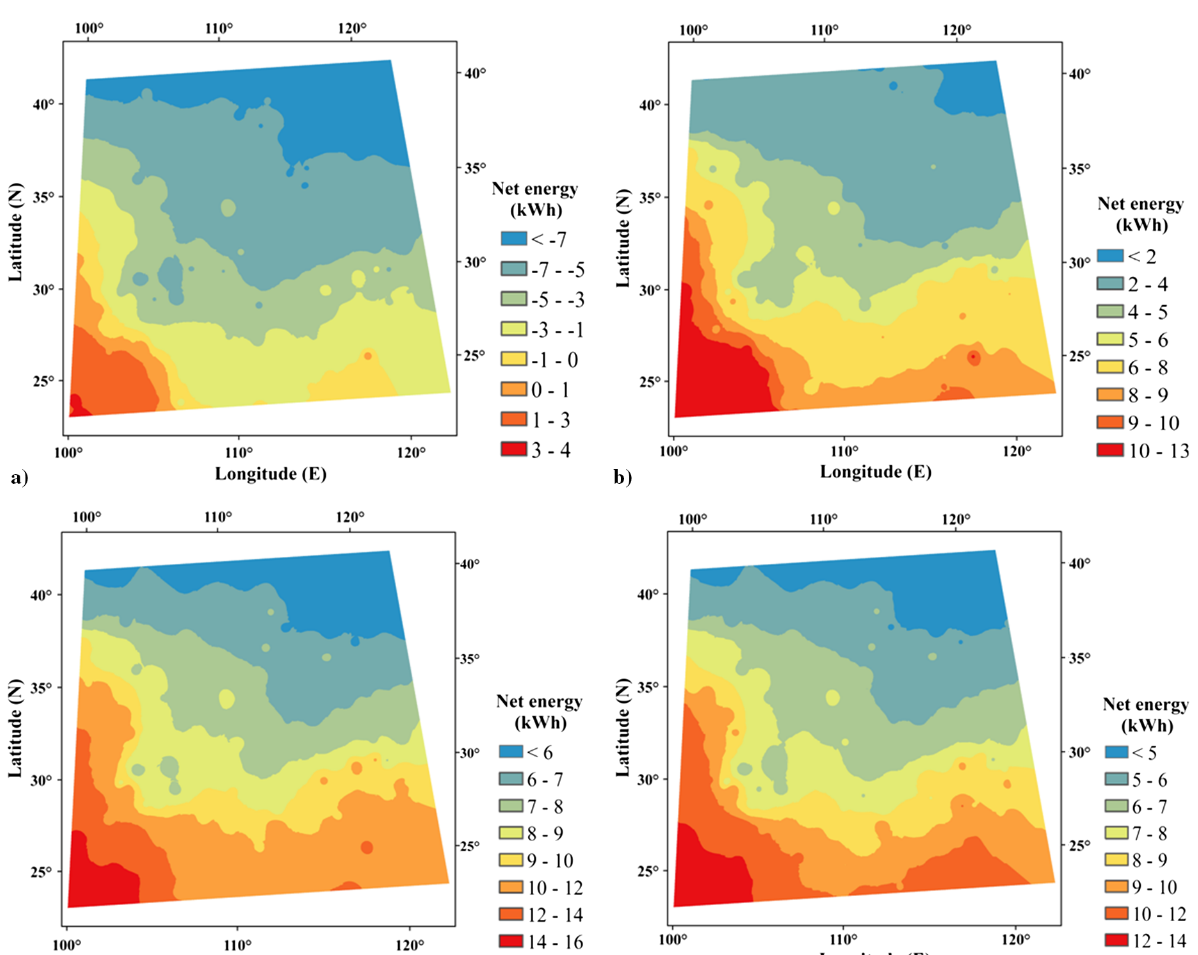

Fig. 3 Endurance maps on January 1, 2018. a) Flight altitude: 10 km; b) flight altitude: 15 km; c) flight altitude: 20 km; and d) flight altitude: 25 km.

III. Results and Discussion

For the simulation, the solar cell and SA configuration parameters are specified as in Table 1, and the initial mission parameters are specified as in Table 2. To examine and discuss the influences of the season and flight altitude on the SA endurance performance, multiple dates and flight altitudes are selected. The endurance maps of the area (longitude range: 100–122°E; latitude range: 23–41.4°N) which belongs to the mission area specified in Table 2 at different flight altitudes on January 1, 2018, and March 21, 2018, are shown in Figs. 3 and 4, respectively.

Remark 3: The SA energy model and corresponding endurance map are closely related to the SA configuration. Consequently, different types of SA for the same mission may result in different endurance maps.

Remark 4: The plotted endurance map can be flexibly selected as the sub-area of the specified mission area.

According to the obtained endurance maps, the qualitative evaluation can be made about whether the mission area is suitable for SA long-endurance flights, and the related distribution rules can be further analyzed. With an increase in the flight altitude, the drag and its energy consumption decrease, while the solar cell efficiency and related energy production remain relatively high. Hence, the net energy first increases. When the flight altitude exceeds 20 km, the solar cell efficiency continuously declines with the increasing altitude. Hence, the net energy decreases later.

With regard to the net energy distribution characteristics, the net energy distribution is largely in line with the trend that the net energy increases with the decreasing latitude. Moreover, compared with the corresponding legends of Figs. 3 and 4, the net energy level increases over the area in the endurance map with an increase in the time. This net energy distribution is in accordance with the solar radiation characteristics of the Northern Hemisphere when the location at which solar radiation is perpendicularly incident at the Earth surface moves from the Southern Hemisphere (January 1) to the Equator (March 21) [17,21].

In addition to the above qualitative analysis and evaluation, the applications of the proposed endurance map can be extended to SA flight mission planning. Two typical examples are shown below.

A. Application 1: Designing the Cross-Regional Horizontal Flight Trajectory

An important application of cartography in the field of aviation is the design of flight trajectories. For SAs, the energy index is crucial; therefore, SAs should fly as far as possible along the area characterized by the higher net energy within the proposed endurance map. For instance, suppose that an SA is flying in steady-state cruise mode along one of two horizontal trajectories, whose lengths are approximately equal, from point A to B, as shown in Fig. 5. It is obvious that the area covered by trajectory 1 exhibits a greater net energy. Therefore, using the endurance map, the energy-optimal trajectory can be intuitively designed to guarantee a sufficient supply of solar energy for an SA cross-regional flight mission.

B. Application 2: Designing the SA Energy Management Strategy and Related 3D Flight Trajectory

To better use the available energy, SAs can adopt some energy management strategies in the cross-regional flight. The most typical strategy is to execute variable-altitude flight to store and release gravitational potential energy at the appropriate time, which involves the design of 3D flight trajectories [1,7,8,11,12]. In contrast to the above-mentioned horizontal trajectory optimization, when designing the SA energy management strategy and corresponding energy-

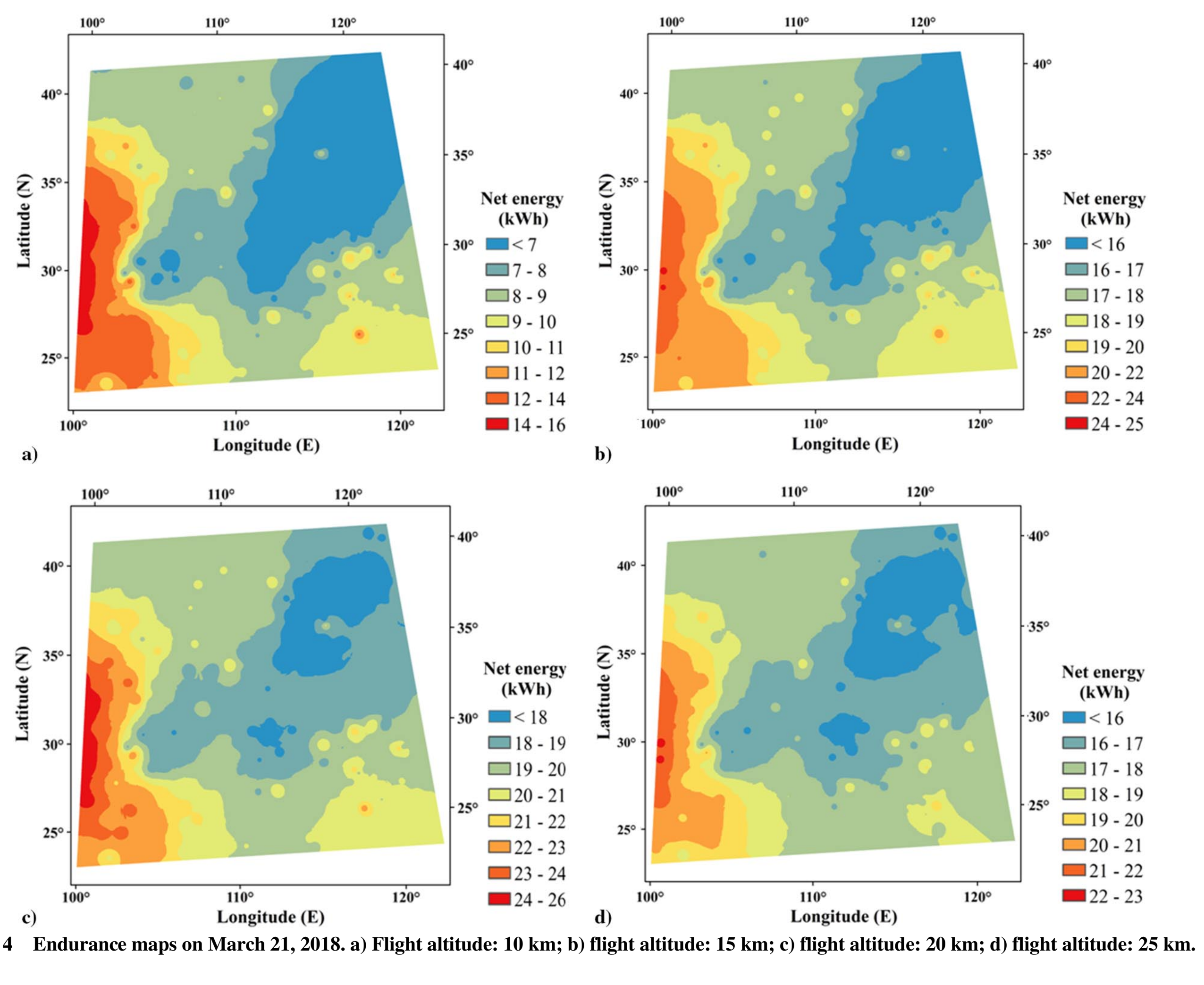

Fig. 4 Endurance maps on March 21, 2018. a) Flight altitude: 10 km; b) flight altitude: 15 km; c) flight altitude: 20 km; d) flight altitude: 25 km.

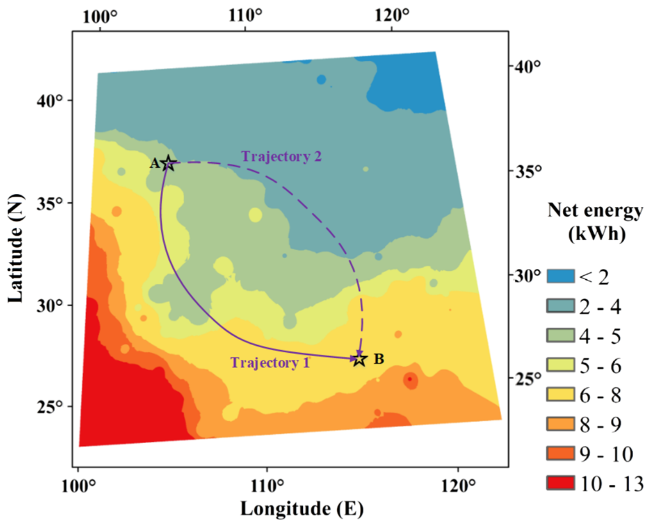

Fig. 5 Schematic diagram for the design of the cross-regional horizontal flight trajectory.

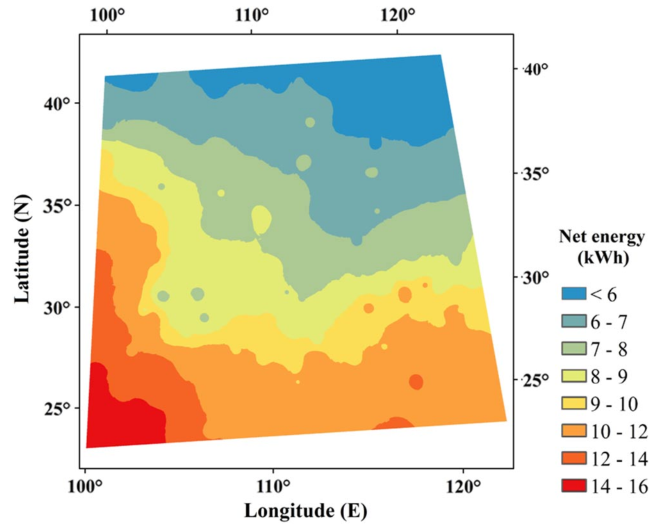

Fig. 7 Absolute optimal net energy distribution map on January 1, 2018.

optimal 3D trajectory, energy distributions are different at different geographic locations, while even at the same location, net energy conditions vary due to altitude. Therefore, during the 3D trajectory design, both the horizontal geographic location and the flight altitude must be simultaneously considered, resulting in a higher complexity.

Based on the concept and methodology of the proposed endurance map, the optimal energy distribution map for the 3D flight can be further derived as follows. First, the energy-optimal flight altitude distribution map should be plotted according to the following steps:

Step 1: For each sampling site, the net energy is obtained at intervals of 100 m within the entire flight altitude range using the ergodic calculation.

Step 2: The flight altitude with the maximum net energy is obtained.

Step 3: Using Kriging interpolation, the energy-optimal flight altitude distribution map is constructed.

The energy-optimal flight altitude distribution map on January 1, 2018, is constructed as shown in Fig. 6, in which the energy-optimal flight altitude is only for a single sampling site. However, the net energy of a site at its optimal altitude may not exceed the net energies of the other sites at their nonoptimal altitudes. Thus, on the basis of the energy-optimal flight altitude distribution map, the differences in the net energy among different sites must also be considered like Application 1. In the process of plotting Fig. 6, the maximum net energy value and the corresponding optimal flight altitude at each site can be obtained, and then Kriging interpolation is used for the maximum net energy values to obtain the absolute optimal net energy distribution map, as shown in Fig. 7. Based on Figs. 6 and 7, the SA variable-altitude flight strategy can be designed as follows:

Step 1: According to the absolute optimal net energy distribution map shown in Fig. 7, the horizontal locations with the higher optimal net energies are designed as the horizontal locations of planned waypoints.

Step 2: According to the planned horizontal locations, the related flight altitudes based on Kriging interpolation are matched using the energy-optimal flight altitude distribution map as shown in Fig. 6.

Step 3: Combined with the planned horizontal locations and the matched altitudes, the 3D flight trajectory is obtained.

Suppose that the planned horizontal locations are marked as A, B, C, D, and E in turns. The 3D flight trajectory in the optimal energy distribution map is obtained as Fig. 8.

IV. Future Work

Future work will be focused on the following aspects:

1) Autonomous 3D trajectory optimization methods and energy management strategies based on the endurance map should be further explored.

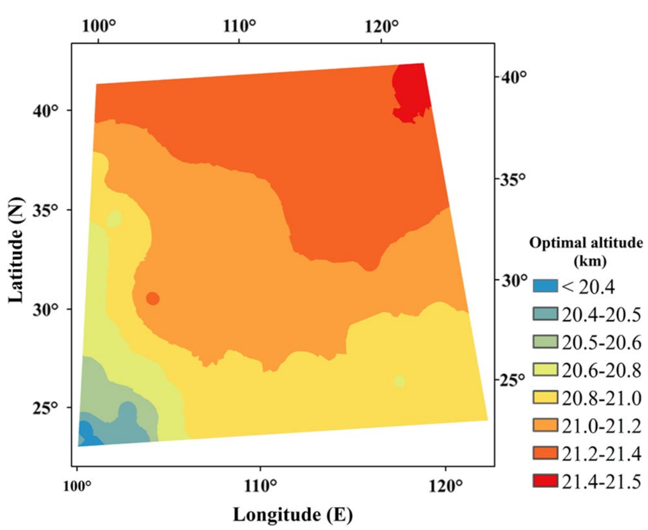

Fig. 6 Energy-optimal flight altitude distribution map on January 1, 2018.

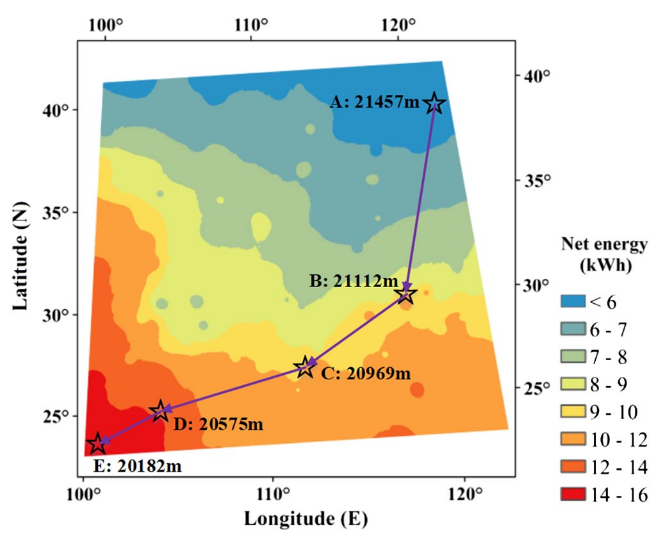

Fig. 8 Schematic diagram for the design of the cross-regional 3D flight trajectory. The corresponding optimal altitudes are marked in this figure.

2) The ASHRAE Clear Sky Model and other mainstream solar irradiance models [31] are mostly based on the radiation data observed at ground level. These data can be influenced by the attenuation due to air humidity. When the air humidity is low, high-altitude solar radiation estimates derived from ground observation data are relatively precise. However, in the summer, the air humidity over some parts of coastal regions and inland basins is relatively high, resulting in a degree of errors within derived high-altitude solar radiation estimates. Therefore, to further improve the precision of the endurance map, future investigations should focus on the modeling and real data accumulation of global high-altitude solar radiation, which are relatively lacking in current studies on solar engineering.

3) In conditions permitting, the experiment validation should be attempted in the future. For this purpose, the software implementation for the endurance map, integrated with the functions of trajectory optimization and energy management, is in development.

V. Conclusions

To address the SA endurance evaluation problem, the concept of an endurance map is proposed for the first time. The 24-hour flight net energy is designed as the evaluation index of the SA endurance performance. Then, the ASHRAE Clear Sky Model is used for energy modeling. Moreover, considering the influences of changes in the geographical location and external environmental factors on the SA endurance performance in the cross-regional flight mission, a variable solar cell efficiency is introduced into the net energy calculation. Finally, Kriging interpolation is used to construct the endurance map, which can visually reflect the endurance performance. The proposed SA endurance map can be used not only to qualitatively evaluate the SA endurance in the mission area but also to design the SA cross-regional flight trajectory and energy management strategy.

Acknowledgments

This research was supported by the National Natural Science Foundation of China under Grants 61673042 and 61803223, the Program for Changjiang Scholars and Innovative Research Team in University under Grant IRT 13004, and the Graduate Innovation Practice Foundation of Beihang University under Grant YCSJ-01-2018-11. The authors would also like to thank the reviewers and the editor for their comments and suggestions that helped to improve the paper significantly.

References

[1] Zhu, X., Guo, Z., and Hou, Z., "Solar-Powered Airplanes: A Historical Perspective and Future Challenges," *Progress in Aerospace Sciences*, Vol. 71, Nov. 2014, pp. 36–53. doi:10.1016/j.paerosci.2014.06.003

[2] Miura, R., and Suzuki, M., "Preliminary Flight Test Program on Telecom and Broadcasting Using High Altitude Platform Stations," *Wireless Personal Communications*, Vol. 24, No. 2, 2003, pp. 341–361. doi:10.1023/A:1022507025134

[3] Gonzalo, J., López, D., Domínguez, D., García, A., and Escapa, A., "On the Capabilities and Limitations of High Altitude Pseudo-Satellites," *Progress in Aerospace Sciences*, Vol. 98, April 2018, pp. 37–56. doi:10.1016/j.paerosci.2018.03.006

[4] Solar Impulse, "Solar Impulse," Nov. 2003, http://www.solarimpulse.com/ [retrieved 10 Aug. 2018].

[5] Ross, H., "Fly Around the World with a Solar Powered Airplane," *The 26th Congress of International Council of the Aeronautical Sciences and 8th Aviation Technology, Integration, and Operations Conference*, AIAA Paper 2008-8954, 2008. doi:10.2514/6.2008-8954

[6] Klesh, A. T., and Kabamba, P. T., "Solar-Powered Aircraft: Energy-Optimal Path Planning and Perpetual Endurance," *Journal of Guidance, Control, and Dynamics*, Vol. 32, No. 4, 2009, pp. 1320–1329. doi:10.2514/1.40139

[7] Hosseini, S., and Mesbahi, M., "Energy-Aware Aerial Surveillance for a Long-Endurance Solar-powered Unmanned Aerial Vehicles," *Journal of Guidance, Control, and Dynamics*, Vol. 39, No. 9, 2016, pp. 1980–1993. doi:10.2514/1.G001737

[8] Gao, X., Hou, Z., Guo, Z., and Chen, X., "Reviews of Methods to Extract and Store Energy for Solar-Powered Aircraft," *Renewable and Sustainable Energy Reviews*, Vol. 44, April 2015, pp. 96–108. doi:10.1016/j.rser.2014.11.025

[9] Wu, J., Wang, H., Li, N., Yao, P., Huang, Y., Su, Z., and Yu, Y., "Distributed Trajectory Optimization for Multiple Solar-Powered UAVs Target Tracking in Urban Environment by Adaptive Grasshopper Optimization Algorithm," *Aerospace Science and Technology*, Vol. 70, Nov. 2017, pp. 497–510. doi:10.1016/j.ast.2017.08.037

[10] Wu, J., Wang, H., Li, N., Yao, P., Huang, Y., and Yang, H., "Path Planning for Solar-Powered UAV in Urban Environment," *Neurocomputing*, Vol. 275, Jan. 2018, pp. 2055–2065. doi:10.1016/j.neucom.2017.10.037

[11] Lee, J. S., and Yu, K. H., "Optimal Path Planning of Solar-Powered UAV Using Gravitational Potential Energy," *IEEE Transactions on Aerospace and Electronic Systems*, Vol. 53, No. 3, 2017, pp. 1442–1451. doi:10.1109/TAES.2017.2671522

[12] Gao, X., Hou, Z., Guo, Z., Liu, J., and Chen, X., "Energy Management Strategy for Solar-Powered High-Altitude Long-Endurance Aircraft," *Energy Conversion and Management*, Vol. 70, June 2013, pp. 20–30. doi:10.1016/j.enconman.2013.01.007

[13] Traub, L. W., "Range and Endurance Estimates for Battery-Powered Aircraft," *Journal of Aircraft*, Vol. 48, No. 2, 2011, pp. 703–707. doi:10.2514/1.C031027

[14] Abdilla, A., Richards, A., and Burrow, S., "Power and Endurance Modelling of Battery-Powered Rotorcraft," *2015 IEEE/RSJ International Conference on Intelligent Robots and Systems (IROS)*, IEEE, New York, 2015, pp. 675–680. doi:10.1109/IROS.2015.7353445

[15] Traub, L. W., "Optimal Battery Weight Fraction for Maximum Aircraft Range and Endurance," *Journal of Aircraft*, Vol. 53, No. 4, 2016, pp. 1177–1179. doi:10.2514/1.C033416

[16] Gatti, M., Giulietti, F., and Turci, M., "Maximum Endurance for Battery-Powered Rotary-Wing Aircraft," *Aerospace Science and Technology*, Vol. 45, Sept. 2015, pp. 174–179. doi:10.1016/j.ast.2015.05.009

[17] Rajendran, P., and Smith, H., "Implications of Longitude and Latitude on the Size of Solar-Powered UAV," *Energy Conversion and Management*, Vol. 98, July 2015, pp. 107–114. doi:10.1016/j.enconman.2015.03.110

[18] Colas, D. F., Roberts, N. H., and Suryakumar, V. S., "HALE Multidisciplinary Design Optimization Part I: Solar-Powered Single and Multiple-Boom Aircraft," *2018 Aviation Technology, Integration, and Operations Conference*, AIAA Paper 2018-3028, 2018. doi:10.2514/6.2018-3028

[19] Montgomery, S., and Mourtos, N., "Design of a 5 Kilogram Solar-Powered Unmanned Airplane for Perpetual Solar Endurance Flight," *49th AIAA/ASME/SAE/ASEE Joint Propulsion Conference*, AIAA Paper 2013-3875, 2013. doi:10.2514/6.2013-3875

[20] Burton, M. J., and Hoburg, W. W., "Solar-Electric and Gas Powered, Long-Endurance UAV Sizing via Geometric Programming," *18th AIAA/ISSMO Multidisciplinary Analysis and Optimization Conference*, AIAA Paper 2017-4147, 2017. doi:10.2514/6.2017-4147

[21] Huang, Y., Wang, H., Li, N., and Yu, Y., "Endurance Estimate for Solar-Powered Unmanned Aerial Vehicles," *2017 9th International Conference on Intelligent Human-Machine Systems and Cybernetics (IHMSC)*, IEEE, New York, 2017, pp. 66–70. doi:10.1109/IHMSC.2017.22

[22] Bergman, T. L., Lavine, A. S., Incropera, F. P., and DeWitt, D. P., *Fundamentals of Heat and Mass Transfer*, 7th ed., Wiley, New York, 2011, Chap. 12.

[23] Oliver, M. A., and Webster, R., "Kriging: A Method of Interpolation for Geographical Information Systems," *International Journal of Geographical Information System*, Vol. 4, No. 3, 1990, pp. 313–332. doi:10.1080/02693799008941549

[24] Retchless, D. P., and Brewer, C. A., "Guidance for Representing Uncertainty on Global Temperature Change Maps," *International Journal of Climatology*, Vol. 36, No. 3, 2016, pp. 1143–1159. doi:10.1002/joc.2016.36.issue-3

[25] Cui, L., Shi, J., Ma, Y., and Du, H., "Distribution and Trend in the Thermal Growing Season in China During 1961–2015," *Physical Geography*, Vol. 38, No. 6, 2017, pp. 506–523. doi:10.1080/02723646.2017.1344497

[26] ASHRAE, *2013 ASHRAE Handbook: Fundamentals (IP & SI)*, ASHRAE, Atlanta, May 1995, https://www.ashrae.org/ [retrieved 14 Oct. 2017].
[27] Goswami, D. Y., *Principles of Solar Engineering*, 3rd ed., CRC Press, New York, 2015, Chap. 2.
doi:10.1201/b18119
[28] Durisch, W., Urban, J., and Smestad, G., "Characterisation of Solar Cells and Modules Under Actual Operating Conditions," *Renewable Energy*, Vol. 8, Nos. 1–4, 1996, pp. 359–366.
doi:10.1016/0960-1481(96)88878-1
[29] Haws, T. D., and Bowman, W., "Thermal Analysis of the Pathfinder Aircraft," *37th Aerospace Sciences Meeting and Exhibit*, AIAA Paper 1999-0735, Jan. 1999.
doi:10.2514/6.1999-735
[30] Staicovici, M. D., *Coabsorbent and Thermal Recovery Compression Heat Pumping Technologies*, 1st ed., Springer, Berlin, 2014, pp. 157–159.
doi:10.1007/978-3-642-54684-6
[31] Ahmad, M. J., and Tiwari, G. N., "Solar Radiation Models—A Review," *International Journal of Energy Research*, Vol. 35, No. 4, 2011, pp. 271–290.
doi:10.1002/er.1690